

## The effect of aluminium additive on the electrical properties of ZnO varistors

A. GUBAŃSKI<sup>1</sup>, W. MIELCAREK<sup>2\*</sup>, K. PROCIÓW<sup>2</sup>, J. WARYCHA<sup>2</sup>, J. M. WRÓBEL<sup>3</sup>

<sup>1</sup>Institute of Electrical Engineering Fundamentals, Wrocław University of Technology,  
Wybrzeże Wyspiańskiego 27, 50-370 Wrocław, Poland

<sup>2</sup>Electrotechnical Institute, Division of Electrotechnology and Materials Science,  
ul. M. Curie-Skłodowskiej 55–61, 50-369 Wrocław, Poland

<sup>3</sup>University of Missouri – KC, Department of Physics,  
5100 Rockhill Rd., Kansas City, MO 64110 USA

Reliable and undisturbed operation of electric and electronic circuits is mainly achieved through the use of appropriate overload protection elements such as overvoltage surge arrestors. The stability of metal oxide varistors which are used insures that the circuits are adequately protected. The point of adding the varistor material with aluminium is the extension of the nonlinearity of  $I$ - $V$  characteristic in high current region. In this work, both the aluminium doping for ZnO varistors, and the effect of this doping on the ageing processes in varistors were investigated. The current trend towards the production of better and more robust surge arrestors which utilize mainly ZnO varistors motivated these studies. The fundamental technological impediments include the repeatability of manufactured varistors and their susceptibility to ageing factors such as current shocks, elevated operation temperature and the extended effect of the operation potential. Improving the varistor imperviousness to ageing continues to be an imperative but, as yet, unsolved problem.

Key words: *ZnO varistors; Al additive; ageing; I-V characteristics; TSDC; nonlinearity exponent*

### 1. Introduction

In order to reduce the destructive effect of overvoltage in power networks, surge arresters are used. These circuits utilize varistors, meaning resistors with variable resistance (variable resistor – VR). Currently, varistors are widely used in both electronic circuits and power networks, often protecting costly devices or an entire installations. Those used in low power devices resemble small parallel-plate capacitors.

---

\*Corresponding author, e-mail: mielcar@iel.wroc.pl

Varistors used in high power equipment have a cylindrical shape, are tens of millimetres in diameter, and are encapsulated in ceramic, epoxy or silicone pipe enclosures.

Varistor fabrication technology has undergone continuous transformation. This progress is stimulated by the desire to lower production costs and improve quality. Lowering the exploitation costs through better protection against failures provides a strong argument for the undertaking the research into varistor technology.

To have varistors working within their specifications is particularly important in exploitation of power networks. Low production costs and a high level of protection has increased the range of varistor applications. The first sintered ceramic varistors were made from silicon carbide (SiC). In the seventies, they were replaced by metal oxide varistors (MOV). Nowadays, oxide based varistors serve as arrestors in a wide range of voltage – from just a few volts to hundreds of thousands of volts [2]. They exhibit strong non-linear current dependence on voltage and are capable of absorbing large quantities of surge energy. Compared to other circuit protection systems such as electronic circuits, they are less expensive and simpler to construct making them more reliable. However, in order to market them effectively, their parameters must be repeatable and fall within precisely specified limits. Understanding and controlling the effects which occur in varistor ceramics, exceeds the range of a single discipline. Current research on this subject is focused on the problem of the conduction mechanisms, the role of the impurities and on the degradation processes. A typical (non-linear) voltage–current ( $V$ – $I$ ) characteristic of a varistor [3] is presented in Fig. 1. The principle of varistor operation is that a raise of the voltage across a varistor above the nominal value, causes an abrupt increase in the overflow current and limits further increase in the voltage.

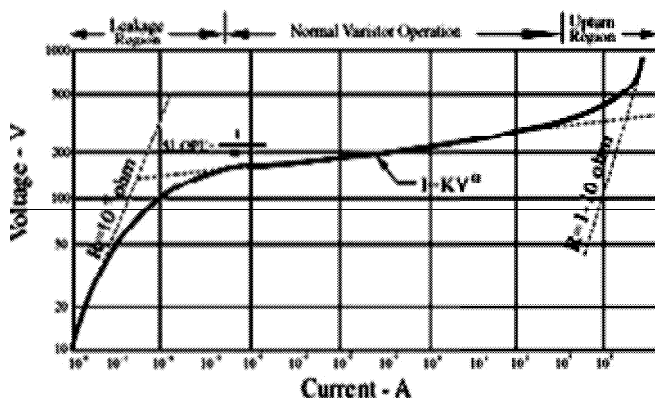


Fig. 1. The voltage–current characteristic of a typical varistor

Three distinct operation regions on the  $V$ – $I$  characteristic exist; a leakage region (A), conduction (voltage clamping) region (B) and upturn (saturation) region. In the leakage region, the resistance of the varistor is in the gigohm range and the current value at the applied working voltage is of the order of microamperes. The mechanisms responsible for the operation of ZnO varistors are described below.

The currents associated with thermal emission of electrons across the Schottky potential barrier dominate varistor conductivity in the leakage region. The temperature affects strongly the shape of the  $V$ – $I$  characteristic in this region. For a single barrier, an exponential function describes the relation between the current density  $J$  and electric field strength  $F$  [1]:

$$J = J_0 \exp\left(\frac{E_b - \beta F^{1/2}}{kT}\right) \quad (1)$$

where  $J_0$  is a current constant,  $\beta$  is the proportionality coefficient,  $k$  is the Boltzmann constant,  $E_b$  is the height of the Schottky barrier, and  $T$  is the operation temperature of the varistor.

In the conduction region, varistors reveal their surge protective properties. They become low resistance devices. This part of the  $V$ – $I$  characteristic can be described by the following exponential dependence

$$I = kV^\alpha \quad (2)$$

where  $k$  is a ceramic constant dependent on the type of the varistor, the nonlinearity exponent  $\alpha$  represents the slope of the characteristic on the double logarithmic scale

$$\alpha = \frac{\log\left(\frac{I_2}{I_1}\right)}{\log\left(\frac{V_2}{V_1}\right)} \quad (3)$$

with arbitrary currents  $I$  and the corresponding voltages  $V$  from this operation region. The nonlinearity exponent of metal oxide varistors a few orders of magnitude exceeds that of carborundum varistors (based on silicon carbide SiC). Depending on the fabrication technology its value may reach 80.

Finally, the upturn region is characterized by a rise in dynamic varistor voltage in line with the current. It is caused by an increase in the resistivity of ZnO grains related to the saturation of free charge carrier concentration. The resistance of the varistor is small (1–10  $\Omega$ ) and relation between current and voltage is again linear.

The individual operation regions of varistors correspond to the current ranges occurring under real conditions. The operational voltages and the dynamic overvoltages fall into the leakage region (A). The switching overvoltages correspond to the conduction region (B). Supervoltages in the upturn region (C) may be caused by lightning surges.

The tendency of varistors to deteriorate resulting in a rise of the leakage current and asymmetry of the  $V$ – $I$  characteristics are the major faults of these devices. They are caused by varistor operation at elevated temperatures as well as overvoltage spikes [4–6]. As surge arrestors, varistors should be reliable and maintain their originally

declared specifications over an extended period of time. ZnO varistors are designed and manufactured for specific work conditions described by maximum (continuous) operation voltage  $V_c$ , nominal surge varistor voltage  $V_n$ , nominal surge current  $I_n$ , and the expected shunt current. Exceeding these values during exploitation may result in the failure of the arrester. In particular, it puts the varistor at risk of degradation. In most cases, it leads to a rise of the leakage current resulting in self-heating of the varistor caused by excess power released in the device. Due to a positive value of the thermal coefficient of conductivity of metal oxide ceramics [7], a heat induced discharge may occur. In more drastic situations, ceramics may break or melt and a surface discharge may occur.

The common reasons for varistor degradation and failures due to ageing include:

- working voltage exceeding the maximum operation value (dynamic overvoltage and ground fault),
- lightning surge current which significantly exceeds the nominal surge current,
- current spikes,
- prolonged overvoltage,
- elevated temperature,
- environmental factors such as ozone, nitrogen oxides, humidity, and pressure.

For a continuous and high level protections of the electric devices provided by arresters, the varistors must exhibit repeatable characteristics and be stable throughout the entire exploitation period. Usually this requires that any change in the varistor characteristic voltage  $V_{1 \text{ mA}}$  (which is a voltage at which the current flowing in the varistor has the value of 1 mA [7]), caused by the earlier listed ageing factors, does not exceed 10% of its initial value.

## 2. Sample preparation

The composition of the material used to prepare the samples for characterization is given in Table 1. Materials of analytical purity were used for manufacturing the samples.

Table 1. Composition of the varistor

Compound	Content [wt. %]
$\text{Bi}_2\text{O}_3$	1
$\text{Sb}_2\text{O}_3$	1
$\text{Co}_2\text{O}_3$	0.5
$\text{MnO}$	0.5
$\text{NiO}$	0.8
$\text{Cr}_2\text{O}_3$	0.4
$\text{ZnO}$	95.8

The processing included milling, mixing and homogenization, drying, granulation, pressing, sintering (1250 °C for 1 h), deposition of the electrodes, and packaging. The prepared varistors were 12 mm in diameter and 2 mm thick. Hydrogenated aluminium

nitrate ( $\text{Al}(\text{NO}_3)_3 \cdot 9\text{H}_2\text{O}$ ) mixed with ground ZnO powder was used for the aluminium doping of the varistor mass. The doping levels, as well as the dimensions of the samples prepared in this process, are listed in Table 2.

Table 2. Aluminium content and the parameters of the investigated samples

No.	Diameter [mm]	Thickness [mm]	Al content	
			[ppm]	[g]
1	12	2.40	0	0
2	12	2.42	12	0.001
3	12	2.38	24	0.002
4	12	2.18	48	0.004
5	12	2.18	96	0.008
6	12	2.26	192	0.016

### 3. Experimental

Varistor samples were placed in a heat chamber, and a laboratory made system for the investigation of passive elements was utilized. The system allows experiments to be carried out at both constant and pulsed currents at maxima of 2 kV and 200 A. Computer controlled, METEX multimeters were also used to measure the current and voltage.

Two ageing factors were used for provoking the degradation process:

- exposure of the samples to an elevated temperature of 115 °C,
- constant overvoltage resulting in a 50  $\mu\text{A}$  current.

The ageing experiment was carried out over a period of 24 h. Additionally, the stabilized current was maintained in the varistor during the process. The procedure allowed one to preserve the conductive paths within the volume of the varistor.

The system used for thermo-stimulated discharge current (TSDC) measurements is described elsewhere [8]. Before the temperature scan, the sample was cooled in a cryostat to 100 K at a constant electric field. The TSDC spectra were collected with the temperature increasing at a constant rate (4 deg/min) from 100 K to 500 K.

### 4. Results and discussion

The ZnO-based varistor samples were subjected to a series of investigative procedures. The goal of these studies was to determine their properties such as characteristic voltage ( $V_{1\text{ mA}}$ ), nonlinearity exponent,  $I$ - $V$  characteristic curve, relaxation parameters (location and height of the TSDC peaks, and activation energy for individual depolarization processes) obtained in the TSDC measurements. The experimental results ob-

tained from examination of the as-received structures provide a basis for evaluation the influence of aluminium doping on varistors.

The investigations of the  $I$ - $V$  characteristics were carried out using the constant current method. The voltage was normalized to 1 mm thickness of the sample. The results shown in Fig. 2, allow one to determine the parameters of the studied samples. The  $I$ - $V$  curves were used for determination of the nonlinearity exponents in the  $0.1 \mu\text{A}$ – $1 \text{ A}$  current range. In this range, the samples with smaller aluminium concentrations (0 and 12 ppm) reach the highest values of the nonlinearity exponent. A significant drop of this parameter is observed in the samples with 96 and 192 ppm additive concentrations. The investigated current range lies on the boundary between the leakage region and the conduction region, and the effect of the Al additive on the nonlinearity exponent may be related to an increase in the leakage current in the doped samples.

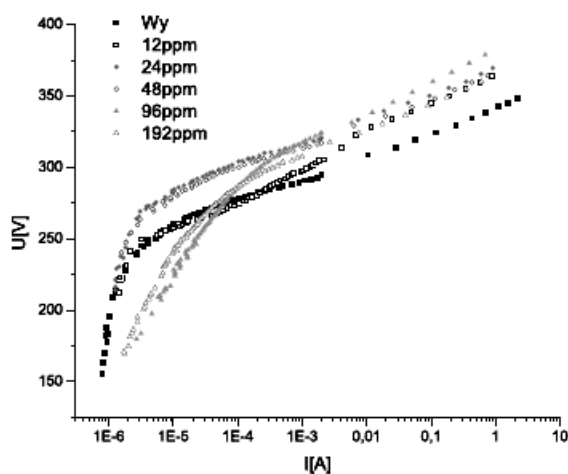


Fig. 2. The  $I$ - $V$  characteristics of brand new varistors with various levels of aluminium doping

A significantly higher leakage current is observed in as-received samples doped at 96 and 192 ppm levels. At 250 V (per 1 mm of sample thickness), the leakage current is greater by a factor of about ten when compared to less doped samples. This implies that aluminium exerts a detrimental influence on the leakage operation region of the varistors. Higher current values cause additional danger associated with selfheating. As seen in Fig. 3, the temperature coefficient of ZnO resistivity is negative, and hence the temperature rise further increases the current. It may eventually initiate the thermal breakdown of the resistor. The nonlinearity exponents found from the  $I$ - $V$  characteristics are listed in Table 3. The results show that for as-received samples, higher aluminium doping reduces the slope of the  $I$ - $V$  characteristic in the leakage region. Comparing the slopes on the  $I$ - $V$  curves for samples with a different concentration of the additive, clearly indicates the undesirable influence of aluminium doping in the leakage region and no effect in the conduction region.

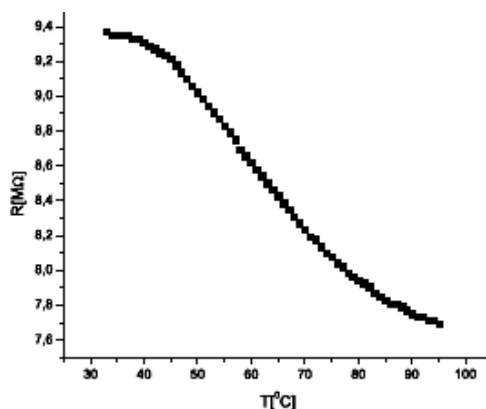


Fig. 3. Temperature dependence of resistance for a ZnO varistor at the stabilized current of 50  $\mu$ A

Table 3. Nonlinearity exponents  $\alpha$  and characteristic voltages  $V_{1 \text{ mA}}$  of as-recived varistor samples obtained from the  $I$ – $V$  characteristics

Al [ppm]	$\alpha$	$V_{1 \text{ mA}}$ [V]
0	42	291
12	33	297
24	42	317
48	44	314
96	36	317
192	39	307

Figure 4 represents typical TSDC spectra for the ZnO varistor cores being investigated. Three well separated peaks ( $\alpha$ ,  $\beta$ , and  $\gamma$ ) appear in the spectra of undoped varistor material as well as in varistor material that has been slightly doped with aluminium (12, 24, 48 ppm). This has been interpreted to mean that the low temperature peak ( $\alpha$ ) may be associated with electron trapping in the layers between the ZnO grains [9]. The next peak ( $\beta$ ) is linked to electron trapping on the donor levels in the depleted region of the Schottky barriers at the grain boundaries. Space charge and ion migration cause the last peak ( $\gamma$ ). Highly doped samples, at the 96 and 192 ppm level, lack the low temperature peak in the TSDC spectrum. This is associated with trapping in the grains and indicates that aluminium additive may influence the relaxation process. The characteristic values of both the current and the temperature for the three spectral features in the TSDC spectrum of brand new samples are listed in Table 4. For purposes of comparison, three calculation methods were utilized in order to determine the activation energies. The initial rise method and the Bucci method [10, 11] yield considerably different values of the activation energy. The discrepancies are caused by the

differences in both the calculation methods and the assumed simplifications. The values obtained are listed in Table 5.

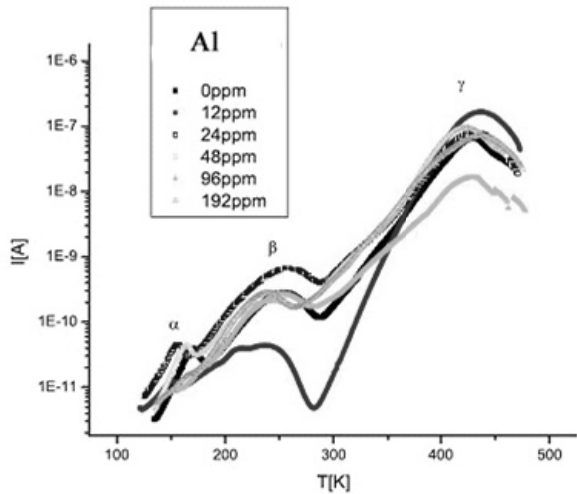


Fig. 4. TSDC spectra for aluminium doped ZnO samples

Table 4. Maxima in the TSDC spectra of as-recived samples and their location on the temperature scale

Al [ppm]	$I_{\max}$ [A]			$T_{\max}$ [K]		
	$\alpha$	$\beta$	$\gamma$	$\alpha$	$\beta$	$\gamma$
0	$3.9\times10^{-11}$	$2.8\times10^{-10}$	$6.6\times10^{-8}$	170	253	428
12	$1.2\times10^{-11}$	$4.4\times10^{-11}$	$1.6\times10^{-7}$	151	237	435
24	$4.5\times10^{-11}$	$6.6\times10^{-10}$	$7.8\times10^{-8}$	157	256	429
48	$4.4\times10^{-11}$	$2.2\times10^{-10}$	$9.5\times10^{-8}$	164	243	420
96	–	$2.6\times10^{-10}$	$1.6\times10^{-8}$	–	251	428
192	–	$2.8\times10^{-10}$	$7.0\times10^{-8}$	–	238	436

Table 5. Activation energies  $E_a$  [eV] determined by the Bucci method, the initial rise method and with the TSDFit computer software

Al [ppm]	TSDFit	BFG	initial rise		
	$\alpha$	$\beta$	$\alpha$	$\beta$	$\gamma$
0	0.59	0.59	0.14	0.12	0.4
12	0.87	0.87	0.04	0.06	0.57
24	0.60	0.60	0.08	0.12	0.26
48	0.50	0.50	0.15	0.10	0.11
96	0.35	0.22	–	0.05	0.14
192	0.43	0.43	–	0.06	0.15



During the ageing processes, variations of the voltage across the varistor were continuously monitored over a 24 h period. Figure 5 represents a typical result for an electrothermally aged varistor. A drop in voltage is observed, confirming the existence of degradation processes in the sample. The removal of the thermal factor yielded a restoration of voltage, meaning that the varistor partially regained its initial properties. In order to find which factor has the decisive influence and what its character is, three samples were exposed exclusively to thermal ageing at the same temperature (115 °C) and over the same time period (24 h). For each sample, the original  $I$ - $V$  characteristics were compared with those obtained after thermal ageing. The curves were identical before and after the process. Hence one can conclude that thermal factor alone does not cause deterioration of the varistor but accelerates degradation caused by the electrical factor.

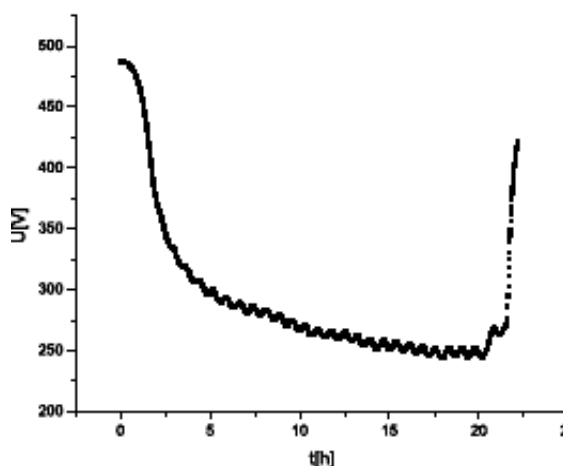


Fig. 5. The time dependency of the voltage across a varistor undergoing an electro-thermal ageing process

After the electrothermal ageing, the sample parameters were investigated again. The purpose of these measurements was to verify the sensibleness of aluminium doping and the influence of the impurities on the degradation processes in ZnO varistors. The measurements of the  $I$ - $V$  characteristics as well as the measurements of the TDSC were carried out. Ageing related changes have been identified. From the  $I$ - $V$  curves, the nonlinearity exponents in the 50  $\mu$ A–1 A range and the characteristic voltages per 1 mm sample thickness were obtained. The values are listed in Table 6. In the undoped sample one can clearly see the effect of ageing on the  $I$ - $V$  characteristic. Significant changes occur in both the leakage region and the conduction region of the varistor. The ageing caused an increase in the leakage current and deterioration of the nonlinearity exponent of the sample. Varistor degradation also increased the resistance of the sample in the conduction region. The aluminium doped samples behaved similarly in the leakage region. After ageing, the leakage current increases noticeably.

However, the degeneration looks different for a greater current. Samples with doping levels of 12, 24, 48 and 192 ppm do not exhibit degenerative changes in the conduction region. The sample doped at the 96 ppm level is an exception showing traces of degeneration in this region. Degradation had no effect on the value of the characteristic voltage. Independent of the doping level, the characteristic voltage remained at the original level after the ageing. Aluminium doping improved the stability of the nonlinearity coefficient. The undoped sample had the largest percentage drop of the nonlinearity coefficient after the ageing. The remaining samples even improved this parameter over their original values. However, there is no proportionality between the percentage changes of the coefficient and the doping level. Samples doped at 12, 48 and 192 have the lowest drop of the nonlinearity exponent due to ageing. The TSDC spectra of the aged varistors show degradation traces through the shift of the low temperature peak toward lower temperatures. The effect of ageing on the activation energies is also noticeable. In the majority of the samples, the activation energy associated with peaks  $\alpha$  and  $\beta$  decreased. Table 7 contains the values of the maxima of TSDC peaks and their locations on the temperature scales before and after the ageing.

Table 6. The nonlinearity exponents and the characteristic voltages per 1 mm of as-recived and aged varistors

Al [ppm]	New sample		Aged sample	
	$\alpha$	$V_{1 \text{ mA}}$ [V]	$\alpha$	$V_{1 \text{ mA}}$ [V]
0	42	291	22	317
12	33	297	31	316
24	42	317	27	317
48	44	314	35	313
96	36	317	21	338
192	38	307	32	304

Table 7. Maxima in the TSDC spectra and the corresponding temperatures

Al [ppm]	$I_{\max}$ [A]			$T_{\max}$ [K]		
	$\alpha$	$\beta$	$\gamma$	$\alpha$	$\beta$	$\gamma$
0	$4.7 \times 10^{-11}$	$3.5 \times 10^{-10}$	$1.1 \times 10^{-7}$	138	257	434
12	$8.3 \times 10^{-13}$	$1.3 \times 10^{-10}$	$1.4 \times 10^{-7}$	135	245	462
24	$4.5 \times 10^{-11}$	$4.3 \times 10^{-10}$	$1.5 \times 10^{-7}$	149	250	454
48	$2.3 \times 10^{-11}$	$1.5 \times 10^{-10}$	$9.2 \times 10^{-8}$	140	243	435
96	—	$4.2 \times 10^{-10}$	$1.6 \times 10^{-7}$	—	245	425
192	—	$1.9 \times 10^{-10}$	$1.5 \times 10^{-7}$	—	244	464

The activation energies of the individual depolarization processes are listed in Table 8. All values were determined using the initial rise method.

Table 8. Activation energies  $E_a$  [eV] corresponding to the individual peaks of the TSDC spectra for as-received and aged samples

Al ppm	As-received sample			Aged sample		
	$\alpha$	$\beta$	$\gamma$	$\alpha$	$\beta$	$\gamma$
0	0.14	0.12	0.4	0.09	0.06	0.2
12	0.04	0.06	0.57	–	0.09	0.31
24	0.08	0.12	0.26	0.1	0.09	0.14
48	0.15	0.1	0.11	0.13	0.7	0.31
96	–	0.05	0.14	–	0.02	0.1
192	–	0.06	0.15	–	0.02	0.09

## 5. Conclusions

Samples exposed exclusively to thermal ageing (115 °C, 24 h) experienced no degradation. Their  $I$ – $V$  characteristics before and after ageing are identical. Only combined electrothermal ageing caused degradation of the samples. In this case, the temperature acted as an initiating and accelerating factor for the electrical ageing process.

Independent of the aluminium content, the ageing process had no effect on the characteristic voltage  $V_{1 \text{ mA}}$  of the investigated varistors. However, the aluminium impurities increased the current values. In the highly doped samples (192 ppm), the currents definitely have larger values.

The largest percentage drop of the nonlinearity exponent occurred in the undoped sample. Nevertheless, because of an increase in the leakage current and a drop in the nonlinearity coefficient, excessive doping levels are undesirable. High doping level also causes that the characteristic voltage  $V_{1 \text{ mA}}$  becomes lower.

Electro-thermal ageing lowers the position of the low-temperature TSDC peak on the temperature scale. Highly doped samples do not exhibit this peak at all.

## Acknowledgements

This work was entirely supported by the Polish Ministry for Scientific Research MNSW under grant No. N N510 344534.

## References

- [1] KOSMAN M.S., PETCSOLD E.G., *O wozmoznosti izgotowlenija simietriczeskich varistorov iz okisi cinka c primiestju okosi bizmuta*, Uczonyje zapiski LGPT im. A.I. Gercena, 207 (1961), 191–196.
- [2] *Harris Semiconductor Transient Voltage Suppression* Products Data book, Harris Corporation 1993.
- [3] MATSUOKA M., Jpn. J. Appl. Phys., 10, (1971), 736.
- [4] EDA K., IGA A., MATSUOKA M., J. Appl. Phys., 51 (1980), 2678.
- [5] JAWORSKI M., WRÓBLEWSKI Z., Przegl. Elektrotechn., 76 (2000), 1.

- [6] PHILIPP H.R., LEVINSON L.M., *Degradation phenomena in zinc oxide varistors – a review*, [In:] *Advances in electronic ceramics*, Vol. 7, *Additives and interfaces in electronic ceramics*, M.F. Yan, A.H. Hener, Columbus, Ohio, Am. Ceram. Soc., 1984, 1–21.
- [7] HOZER L., *Semiconductor Ceramics: Grain Boundary Effects*, Ellis Horwood Ltd., 1994.
- [8] GUBAŃSKI A., MACALIK B., Bull. Acad. Sci., 35 (1987), 537.
- [9] EMTAGE P.R., J. Appl. Phys., 48,(1977), 4372.
- [10] GARLICK G.F.J., GIBSON A.F., Proc. Phys. Soc., 60 (1948), 574.
- [11] BUCCI C., FIESHI R., GUIDI G., Phys. Rev., 148, (1966), 816.

*Received 26 April 2007*

*Revised 14 August 2007*